LBL-21063
Preprint

Lawrence Berkeley Laboratory
UNIVERSITY OF CALIFORNIA

Submitted to Physical Review C

ANGULAR CORRELATIONS BETWEEN PROJECTILE AND TARGET FRAGMENTS EMITTED FROM NUCLEAR COLLISIONS OF ^{238}U AT 0.85 A GeV

H.H. Heckman, Y.J. Karant, and E.M. Friedlander

March 1986

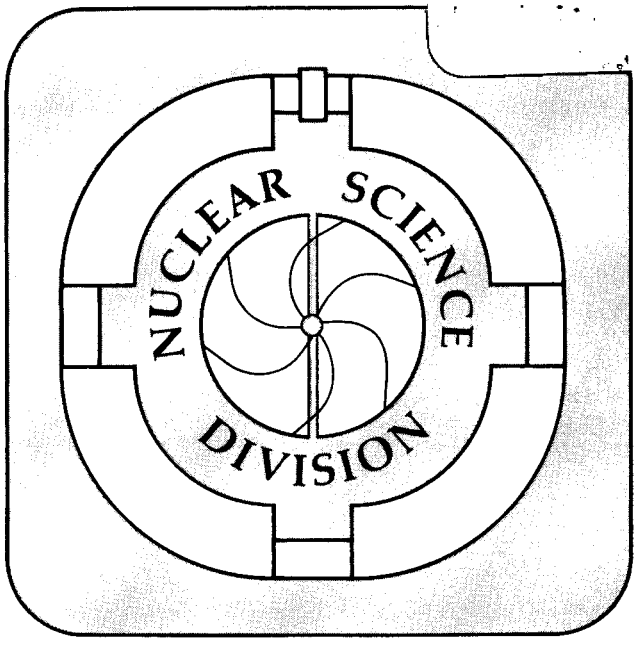

Prepared for the U.S. Department of Energy under Contract DE-AC03-76SF00098

DISCLAIMER

LBL-21063

Angular Correlations Between Projectile and Target Fragments Emitted from Nuclear Collisions of ^{238}U at 0.85 A GeV

H.H. Heckman, Y.J. Karant and E.M. Friedlander

Nuclear Science Division
Lawrence Berkeley Laboratory
University of California
Berkeley, California 94720

This work was supported by the Director, Office of Energy Research, Division of Nuclear Physics of the Office of High Energy and Nuclear Physics of the U.S. Department of Energy under Contract DE-AC03-76SF00098.

LBL-21063

Angular Correlations Between Projectile and Target Fragments Emitted from Nuclear Collisions of ^{238}U at 0.85 A GeV

H.H. Heckman, Y.J. Karant and E.M. Friedlander

Nuclear Science Division
Lawrence Berkeley Laboratory
University of California
Berkeley, California 94720

ABSTRACT

We report measurements on the angular distributions of, and correlation between, projectile and target fragments emitted in high-multiplicity, peripheral collisions of 0.85 A GeV-^{238}U nuclei with Ag(Br) nuclei. The observations are amenable to an interpretation based on elemental two-body kinematics.

This work was supported by the Director, Office of Energy Research, Division of Nuclear Physics of the Office of High Energy and Nuclear Physics of the U.S. Department of Energy under Contract DE-AC03-76SF00098.

Angular Correlations Between Projectile and Target Fragments Emitted from Nuclear Collisions of ^{238}U at 0.85 A GeV

I. INTRODUCTION

An examination of inelastic nuclear interactions of ~1 A GeV-^{238}U nuclei in research emulsions reveals a large range of target/projectile multiplicities, ranging from simple binary fission to complete disintegration of both the uranium projectile and target nucleus into nucleons and light nuclear fragments.[1] A particular class of uranium interactions we have chosen for study are those that exhibit the classical target-/projectile-fragment topologies, selected by the criteria that the interactions occurred at beam energies $0.75 \leq E/A \leq 0.95$ GeV and at least 8 projectile-related fragments ($Z \geq 2$) and 10 target-related fragments ($Z \geq 1$) were produced in the interaction. The last criterion insures that the target nuclei pertain to the high Z nuclei in emulsion, i.e, Ag(Br). The measurements we have carried out were restricted to the multiplicities and angular distributions of both target and projectile fragments. Because of the high multiplicities of both target and projectile fragments, statistically meaningful measurements on the angular correlations between target and projectile fragments become possible on an event-by-event basis.

The motivation for selecting uranium interactions with Ag(Br) nuclei under the above criteria is visually evident from the micro-projection drawing shown in Fig. 1. Here, the 0.92 A GeV ^{238}U beam nucleus enters from the left and collides with a Ag(Br) nucleus to produce an event having high multiplicities of both projectile and target fragments. The projectile fragments (PF) are emitted in a well defined forward cone, but whose mean direction is notably non-collinear with the incident beam nucleus, being deflected downward by about 2° in this event. We point out here that the heaviest element in emulsion, ^{108}Ag, has a geometric cross section $\sigma = 1.4$ b, whereas the cross section of ^{238}U is $\sigma = 2.4$ b. Thus, the ^{238}U projectile can never be fully occulted by a target nucleus in emulsion. Hence, on the basis of a geometric abrasion model there should always be 0°-spectator fragments of the U nucleus. Instead, one sees in this event a void of 0°-projectile fragments ($\theta_{min} = 1.0°$ in this event), and a striking, but typical, deflection of the entire population of PFs, characteristic of a coherent interaction of the U projectile. The low-velocity target fragments (TF) likewise do not have their usual near-isotropy in angle, but exhibit an asymmetric emission pattern characteristic of a moving, particle-emitting system directed opposite to the deflection of the projectile fragments under the dictates of momentum conservation. In this event a reaction plane can be well defined.

Qualitatively, the class of events that is illustrated in Fig. 1 has the collective effects of "bounce-off" of the projectile fragments, and the "side-splash" of the target, i.e. intermediate-rapidity fragments that have been revealed in the energy-flow analysis of the reaction Nb + Nb at 400 A MeV.[2] Collective flow of matter has also been observed in the

exclusive charged-particle spectra observed in the reaction Ar + Pb at 0.77 A GeV, where the sidewards deflections of the momentum flux are attributed to collisions having intermediate (i.e., non-central) impact parameters.[3] Predictions from nuclear fluid dynamics in the angular distribution of the flow angles of fragments produced in multiplicity-selected collisions are in qualitative agreement with experiment.[4]

The purpose of this investigation is therefore: i) to examine the extent to which the event shown in Fig. 1 is characteristic of the selected class of high-multiplicity U + nucleus collisions, and ii) to learn to what extent the angular correlations between that projectile and target fragments, and the angular distributions of the projectile and target fragments emitted in these interactions,are dictated by 2-body kinematics.

II. OPERATIONAL METHODS

Beams:

Two stacks of 600 μm-thick pellicles of Ilford G•5 emulsion, of dimensions 4 x 11 x 1 cm^3 (stack 1) and 7.5 x 12.5 x 1.2 cm^3 (stack 2) were irradiated by 0.96 A GeV-^{238}U nuclei at the Bevalac. The uranium beams entered the stacks parallel to the emulsion surfaces. The range of stopped, non-interacting beam nuclei in the emulsion stacks was 3.05 cm. After grid printing and processing, the emulsions from stack 1 were scanned over the beam profile for a distance of 1 cm from the entrance surface, and in the case of stack 2 were scanned at the entrance edge for entering beam tracks, which were followed until they either interacted or reached their end-of-range. Beam fluences were 1 x 10^3 and 0.2 x 10^3 $cm^2$for stacks 1 and 2, respectively.

Event Selection:

Of a total of 748 interactions detected in the energy interval $0.75 < E/A < 0.95$ GeV, 110, or about 15% of all the interactions with emulsion nuclei fulfilled the criteria that at least 8 projectile-related fragments ($Z \geq 2$) and 10 target-related fragments and ($Z \geq 1$) were produced in the interaction. Of these, 49 events were deemed suitable for measurement on the bases they were not obscured by δ-rays from nearby beam tracks (a significant effect in stack 1 because of high beam-track density) and occurred at distances $\tilde{>}$ 80 μm from either the top or bottom surface of the emulsion pellicle, to permit angle measurements of the emitted fragments over 4π steradian.

Measurements:

Multiplicity and angular distributions were obtained for

i) projectile fragments having $Z \geq 2$, and for

ii) target fragments whose rates of ionization corresponded to $Z = 1$ particles having energies $\lesssim$ 100 A MeV. The ionization rates, i.e. charges, of projectile fragments were classified as having charge $Z \geq 2$ or $Z \geq 6$, estimates that can be made visually to sufficient accuracy in the present experiment.

All emission angles were determined from the vector directions of the incident and emitted tracks determined by measurement of the xyz coordinates of two points along each track. The points of measurement were separated by distances up to ~1 mm, depending on the energy, i.e. multiple scattering, and direction of the emitted fragment. The track coordinates were measured under 1000 X magnification, with microscope-stage readout digitized in 1 μm units. Components of the track vectors parallel to the optical (z-) axis of the microscope, i.e. normal to the emulsion surface, were corrected for the

shrinkage of the processed emulsion pellicle. From these measurements we obtained the distributions of polar (θ) and azimuthal (ϕ) angles of the projectile and target fragments

i) relative to the incident-beam vector, and

ii) relative to their principal vectors of emission, $\hat{r}_{PF}$ and $\hat{r}_{TF}$, respectively, defined below.

Coordinate Frames:

Figure 2a,b defines the coordinate systems we have used. Figure 2a is the "beam" system, where $\underline{i}$ is directed along the momentum vector of the incident beam nucleus, $\underline{j}$ lies in the plane of the emulsion, with $\underline{k} = \underline{i} \times \underline{j}$ being (approx.) normal to the emulsion plane. The polar and azimuthal angles of a fragment in the beam frame are θ and ϕ, respectively. Figure 2b is the "fragment" system, were the $\underline{i}'$ axis is directed along the principal vector of emission, $\hat{r}$, of either the target or projectile fragments, with $\underline{k}' = \underline{i}' \times \underline{j}$. The polar angle θ' of a given fragment-vector $\underline{r}$ in the TF frame is indicated in this figure.

We have defined the principal (unit) vector of emission for N fragments (from either the projectile or target nucleus) to be

$$\hat{r} = \frac{\left(\sum_{\ell=1}^{N} r_x\right)\underline{i} + \left(\sum_{\ell=1}^{N} r_y\right)\underline{j} + \left(\sum_{\ell=1}^{N} r_z\right)\underline{k}}{\left(\sum_{\ell=1}^{N} r_x^2 + \sum_{\ell=1}^{N} r_y^2 + \sum_{\ell=1}^{N} r_z^2\right)^{1/2}} \qquad \text{(Eq.1)}$$

where r_x, r_y and r_z are the components of the unit vector of the $\ell^{\underline{th}}$ fragment.

The azimuthal and polar angles of the vector $\hat{r}$ for N fragments are defined to be:

i) azimuth : $\phi = \tan^{-1}(\hat{r} \cdot \underline{k}/\hat{r} \cdot \underline{j})$ (Eq.2)

and ii) polar : $\theta = \cos^{-1}(\hat{r} \cdot \underline{i})$. (Eq.3)

III. RESULTS

Multiplicities:

Figure 3 gives the scatter plot of multiplicities of the projectile and target fragments of the selected events. The average multiplicity for the projectile fragments, $Z \geq 2$, for events (with $N_{PF} \geq 8$) is $\bar{N}_{PF} = 13.5$ with dispersion $D = 3.6$, and for target fragments ($\bar{N}_{TF} \geq 10$), $\bar{N}_{TF} = 22.7$, with $D = 5.8$. The largest target multiplicity in our sample was 41, which represents the near complete disintegration of an Ag($Z = 47$) target nucleus into $Z = 1$ fragments. The multiplicity of projectile fragments $Z \geq 2$ in this event was $N_{PF} = 16$. The total multiplicity of tracks of 57 was also the largest in the data sample.

Although the events selected for this study exhibit the topology of projectile-fragmentation reactions (i.e. peripheral collisions) it is noteworthy that the mean multiplicity of target fragments, $\bar{N}_{TF} = 22.7$, represents more than 50% of the average atomic number $\bar{Z} = 41$ for Ag(Br), under the unrealistic assumption that all fragments are $Z = 1$. In other words, by restricting our observations to target multiplicities alone, most of the events involve major break-up of the target nucleus, traditionally attributed to "central" collisions when lighter beam nuclei are used and projectile-fragment information is lacking.

Angular Distribution:

A. Principal Vectors. The principal vectors of the projectile and target fragments, $\hat{r}_{PF}$ and $\hat{r}_{TF}$, respectively, were determined for each event via Eq.1. Conceptually, we assume these vectors establish, to good approximation, the momentum vectors, i.e. direction of emission, of the

produced "sources" of the projectile and target fragments. The azimuth and polar angles of the vectors $\hat{r}$ were evaluated from Eq. 2.

1. Azimuthal. Figure 4 presents the differences between the azimuthal angles of the target and projectile vectors, $\Delta = \phi_{TF} - \phi_{PF}$, for each of the 49 events. The data show a strong back-to-back correlation, 47 of the 49 events having Δ in excess of 90°, with a mean difference of $\bar{\Delta} = 146 \pm 4°$ and dispersion $D = 28°$. These data are compared with those derived from a Monte Carlo simulation of the entire data set assuming isotropic emission of the N_{PF} and N_{TF} fragments observed for each event. The calculated distribution for $\Delta(MC) = \phi_{TF}(MC) - \phi_{PF}(MC)$, shown in Fig. 4, has a mean $\bar{\Delta}(MC) = 97 \pm 8°$ and dispersion $D = 55 \pm 6°$, compatible with that expected for a uniform distribution, namely 90° and 52°, respectively.

The azimuthal correlations illustrated in Fig. 4 imply significant correlations in the angles of emission of the projectile and target fragments. The observation that the azimuthal directions of $\hat{r}_{TF}$ and $\hat{r}_{PF}$ are, on the average, separated by 146 ± 28° (SD), is indicative of a well-defined reaction plane in this class of U-nucleus events.

2. Polar. The angular distributions $dN/d\theta$ of the principal PF and TF vectors, $\hat{r}_{PF}$ and $\hat{r}_{TF}$, are shown in Fig. 5. The distribution $dN/d\theta$ for the $\hat{r}_{PF}$ vectors, evaluated using all projectile fragments $Z \geq 2$ in the 49 events, is characteristically confined to small angles of deflection, with a mean angle $\bar{\theta}_{PF} = 2.35 \pm 0.20°$. The distribution $dN/d\theta$ for the $\hat{r}_{TF}$ vectors are distributed at larger "recoil" angles, with a mean $\bar{\theta}_{TF} = 47.1 \pm 2.1°$.

In order to search for a dependence of $\bar{\theta}_{PF}$ on selected intervals of θ_{TF}, we evaluated separately $\bar{\theta}_{PF}$ for one-half of the events with

i) $\theta_{TF} \leq \theta_{TF}(\text{median})$, where $\theta_{TF}(\text{med}) = 44.9°$, and ii) $\theta_{TF} > \theta_{TF}(\text{med})$. The angles $\bar{\theta}_{TF}$ and $\bar{\theta}_{PF}$ for these data, and that for the combined data described above, are included in Table I(a).

B. Projectile and Target Fragments. The angular distributions of the projectile (Z = 2) and target fragments, as viewed from their respective PF and TF frames, Fig. 1b, are given in Figs. 6 and 7. In these frames, the angle θ' is the angle of emission of a fragment relative to the principal vector $\hat{r}$, where, as illustrated in Fig. 1b, θ'_{TF} is the angle of a target-fragment vector r in the TF-frame.

Figure 6 is the projected angular distribution $dN/d\theta'_{PF}(\text{proj})$ of Z = 2 projectile fragments, where the angles $\theta'(\text{proj})$ are the projections of $\theta'_{PF} = \cos^{-1}(r \cdot \hat{r}_{PF})$ onto the $(\underline{i}',\underline{j}')$ and $(\underline{i}',\underline{k}')$ planes defined in each event. The distribution of the Z = 2 PFs is gaussian-like, with dispersion D = 3.6° (63 mrad).

Figure 7 presents the observed angular distribution $dN/d\cos\theta'$ of the target fragments (closed circles). The distribution is of exponential form, with a forward-backward ratio F/B = 5.94 ± 0.51. The slope $\underline{b}$ of the line drawn through the data is given by $\underline{b} = \ln(F/B) = 1.78 \pm 0.15$. The observed distribution $dN/d\cos\theta'$, however, must be corrected for the inherent bias (spurious asymmetry) introduced when the empirically-determined vector $\hat{r}_{TF}$ is chosen as the angular origin. This inherent asymmetry was evaluated by a Monte Carlo (MC) simulation of each event of the data set, assuming an anistropic distribution of the form $dN/d\cos\theta' \propto \exp(\underline{b}\cos\theta')$ [see Eq. 6]. The results of the MC calculations, based on twenty repetitions of the data set (2.222×10^4 tracks), showed that the asymmetry introduced by choosing $\hat{r}_{TF}$ as the origin, while not altering the

exponential form of the distribution, systematically increases the F/B ratio of the distribution by factors $f = (F/B_{obs} : F/B_{corr}) > 1$. The factor f varies from $f = 1.78 \pm 0.02_5$ for an isotropic distribution, i.e. $F/B_{corr} = 1$, to $f = 1.125 \pm 0.024$ for anisotropic distributions having intrinsic F/B_{corr} ratios in the range 5 to 7, ratios that encompass the values observed in this experiment. Thus, the corrected F/B ratio for the observed angular distribution shown in Fig. 7 is $F/B_{corr} = f^{-1}(F/B_{obs}) = 5.28 \pm 0.46$. Drawn in Fig. 7 as a dashed line is the input (corrected) distribution with slope $\underline{b} \equiv \ell n(F/B_{corr}) = 1.66$ which was used to generate by MC simulation the observed angular distribution with $F/B_{obs} = 5.94$.

Similarly, the F/B_{corr} ratios were determined for those events in which i) $\theta_{TF} \leq \theta_{TF}(med)$ and ii) $\theta_{TF} > \theta_{TF}(med)$. The values of F/B_{corr} for these data are listed in Table I(a).

IV. ANALYSIS

Kinematic properties of the high-multiplicity ^{238}U + Ag(Br) events under consideration that evolve from the observed topological angular distributions of the projectile and target fragments can be summarized as follows:

a) A well-defined reaction plane is characteristic of the interaction, as indicated by the azimuthal correlation between the projectile and target fragments.

b) The $Z \geq 2$ projectile fragments of the incident ^{238}U nucleus are deflected, on the average, between $\bar{\theta}_{PF} = 2°$ to 3° from the beam direction. Under the assumption that $\bar{\theta}_{PF}$ represents a deflection of the primary ^{238}U nucleus, transverse momenta $p_t \approx 15$ GeV/c (60 MeV/c per nucleon) would be a typical value of p_t in the interaction. This value of p_t is comparable

to that observed (≈50 MeV/c per nucleon) for the "bounce-off" projectile fragments in Nb + Nb collisions at 400 MeV/nucleon.[2]

c) Target fragments are emitted at recoil angles of $\bar{\theta}_{TF} = 47 \pm 15°$ (SD). At $p_t \approx 15$ GeV/c, a Ag(Br) target nucleus ($\bar{A} = 94$) at this angle would have a momentum of $p \approx 20$ GeV/c, corresponding to a recoil velocity $\beta \approx 0.2$.

d) For beam-velocity projectile fragments ($\beta\gamma_{beam} = 1.6$) the dispersion of the projected angular distribution of the Z = 2 PFs, D = 3.6°, corresponds to a projected momentum width in the fragmenting nucleus of about 90 MeV/c per nucleon ($\beta\gamma = 0.10$). A characteristic velocity for nucleons in the projectile-fragment system is therefore $\beta \approx \sqrt{3}\ (0.1) = 0.17$.

e) The forward to backward asymmetry of the target fragments relative to their principal vector $\hat{r}_{TF}$ is characteristic of a particle-emitting source moving at velocity $\beta_{||}$ in the direction of $\hat{r}_{TF}$. If we identify $\beta_{||}$ with the target-recoil velocity β qualitatively estimated in c) above, then $\beta_{||} \approx 0.2$.

f) The magnitude of the F/B ratio of particles emitted from a moving source depends upon the ratio of source-velocity $\beta_{||}$ and β_0, the characteristic velocity of the source (see following section). The observed ratios $F/B)_{corr} \approx 5$ imply that the velocities $\beta_{||}$ and β_0 do not differ greatly.

From this synopsis we are led to suggest that the class of high-multiplicity events we have selected are similar to those one might envision to exhibit the "bounce-off, side-splash" phenomena that describe the effects of collective flow observed in the Plastic Ball Nb + Nb experiment at 400 Mev/nucleon.[2] From our observations, the selected events have features that are topologically and kinematically associated with quasi-elastic scattering. We shall find, in fact, that our observations are amenable to an

interpretation based on the kinematics of quasi-elastic scattering. For definiteness, we shall consider the reaction, $^{238}U + {}^{94}A_t \rightarrow {}^{238}U^* + {}^{94}A_t^*$ as representative of our selected events, where A_t represents the average Ag(Br) target nucleus having mass number $\bar{A} = 94$ and charge $\bar{Z} = 41$. We proceed with the elemental kinematics of this reaction.

Kinematics:

Figure 8 shows the recoil angle of a $^{94}A_t^*$ nucleus versus the angle of deflection of the incident 0.85 A GeV ^{238}U-beam nucleus, as a function of the excitation energy E^*(GeV), in the quasi-elastic reaction $^{238}U + {}^{94}A_t \rightarrow {}^{238}U^* + {}^{94}A_t^*$. The calculation is made under the assumption that the (total) excitation energies E^* for the target and projectile nuclei are equal, i.e. the masses of the nuclei are initially given by M = 0.9315 A GeV and, in their excited states, by $M^* = M + E^*$ GeV. Thus, for example, a deflection of 2° of the U projectile will produce an A_t-recoil angle from 85° at $E^* = 0$ GeV (elastic scattering) to 30° at $E^* = 9$ GeV. Plotted in this figure are the three pairs of observed angles $\bar{\theta}_{TF}(\equiv\theta_{A_t}*)$ and $\bar{\theta}_{PF}(\equiv\theta_U*)$, the latter based on all PFs $Z \geq 2$ (Table I(a)). The data are clearly incompatible with elastic scattering. Drawn through each data point is a segment of the kinematic curves for the excitation energies established by these data points. For the composite data sample [circle], the angles $\bar{\theta}_{TF}$ versus $\bar{\theta}_{PF}$ correspond to $E^* \approx 5.8$ GeV; for events with $\theta_{TF} \leq \theta_{TF}$(med) [square], $E^* \approx 7.5$ GeV and for $\theta_{TF} > \theta_{TF}$(med) [triangle], $E^* \approx 4.1$ GeV. The nucleon velocities in the excited U projectile for these values of E^*, $\beta = \sqrt{2E^*/M}$, are in the range $0.19 < \beta < 0.26$, compatible with item IV-d above.

The calculated velocities of the recoiling A_t^* systems for these three cases are in the range $0.20 < \beta_{A_t}* < 0.21$, again compatible with topologically-estimated velocities given in IV.-c. The corresponding range in momentum is $205 < p_{A_t}* < 215$ MeV/c per nucleon. This implies that the momentum transferred to the target nucleus for these classes of events does not depend sensitively on the degree of excitation.

Effects of Coulomb Scattering:

The extent to which coherent Coulomb scattering of the incident U projectile by an Ag(Br) target nucleus contributes to the deflection angle $\bar{\theta}_{PF}$ (=2-3 deg) has been estimated under the following assumptions:

i) The charge of a nucleus is confined to a spherical volume of radius $R = r_0 A^{1/3}$, with $r_0 = 1.4$ fm.

ii) The scattering is considered as a two-step process:

First, the pre-collision transverse impulse imparted to the incident ion at velocity v(lab) and impact parameter b is given by

$$p_t = \int_{-\infty}^{0} F_\perp \frac{dx}{v} = Z_1 Z_2 e^2 / vb \quad .$$

Second, for collisions with $b < R_1 + R_2 \equiv b$ (grazing), the post-collision impulse p_t imparted to the U "spectator" is the sum of the impulses imparted to it by the Coulomb fields of the target-spectator and of the (double-charge density) "fireball" that is comprised of the participant nucleons. The velocity of the fireball relative to the U spectator (at beam velocity β) is given by $\beta_{rel} = (\beta - \beta_{CM})/(1 - \beta\,\beta_{CM})$, where β_{CM} is the center-of-mass velocity of the fireball. For these calculations we have adopted the kinematics of the fireball/spectator model given in Ref. 5.

The results of this calculation give the Coulomb scattering angle of the U spectator in U + Ag(Br) collisions as a function of the impact parameter b. If we associate collisions with an impact parameter in the range $8.9 \leq b \leq 10.6$ fm as giving rise to the class of events selected in this experiment ($0.15\ \sigma_{geom}$)--which follows from the assumptions that collisions with $b \geq 10.6$ fm give rise to fission reactions ($0.50\ \sigma_{geom}$) and those with $b \leq 8.9$ fm give rise to more catastrophic central collisions ($0.35\ \sigma_{geom}$)[1]--then the estimated Coulomb scattering angle of the U spectator at 850 A MeV is $0.26° \lesssim \theta_{Coul} \lesssim 0.37°$. We note that these angles are twice that calculated for grazing collisions, i.e., $\theta_{Coul} = 0.13°$ at $b = 15.0$ fm.

Our conclusion, then, is that Coulomb scattering contributes only about 15% to the observed deflection angle $\bar{\theta}_{PF}$. It follows therefore that the deflection of the U projectile must be attributed primarily to a collective hadronic effect.

Angular Distribution of Target Fragments:

Based on the kinematics of quasielastic scattering considered above, we find that the recoil velocities of the target nucleus are non-relativistic, with kinematic energies typically 15 to 20 A MeV. This leads use to consider the parameterization of the angular distributions of the target fragments in terms of a modified Maxwell-Boltzmann distribution. This distribution, expressed in a non-relativistic form as a function of the momentum per nucleon p of the emitted fragments, with c = 1, is given by:

$$\frac{dN^2}{dp\ d\cos\alpha} \propto p^2 e^{-(p^2 - 2m\beta_{\parallel} p\cos\alpha)/2m\tau} \qquad \text{(Eq.4)}$$

where $\beta_{\parallel}$ is the longitudinal velocity of the particle-emitting system, α is

the laboratory angle between the momenta of a fragment and the particle-emitting system, the latter at temperature τ, and m is the mass of the nucleon (931 MeV). The characteristic particle velocity of the excited system is $\beta_0 = \sqrt{2\tau/m}$.

As shown in Ref. 6, the angular distribution of fragments, $dN/d\cos\alpha$, derived from Eq.4, when measured without regard to fragment velocity (as in the present experiment) becomes a function of the parameter $x_0 = \beta_{||}/\beta_0$ only. In this particular case, the ratio of the number of fragments emitted in the forward to backward direction, F/B, is given by

$$F/B = \frac{1 + \text{erf } x_0}{1 - \text{erf } x_0} \qquad \text{(Eq.5)}$$

To first order in x_0, the angular distribution can be expressed as

$$\frac{dN}{d\cos\alpha} \propto \exp\left[\frac{4}{\sqrt{\pi}} x_0 \cos\alpha\right] \qquad \text{(Eq.6)}$$

In the present application we identify the target-fragment vector $\hat{r}_{TF}$ with the velocity vector of the moving particle-emitting system, with α corresponding to θ', the angle of the target fragment measured with respect to $\hat{r}_{TF}$, as schematically illustrated in Fig. 1b. The ratio x_0, in terms of the non-relativistic recoil and excitation energies of the target nucleus, becomes $x_0 = \sqrt{3T_{A_t}^* /2E^*}$, given the (non-relativistic) relation $E^*/A = \frac{3}{2}\tau$ for the available kinetic energy per nucleon in the target nucleus at temperature τ.

The observed distribution $dN/d\cos\theta'_{TF}$, Fig. 7, is compatible with the (approximate) exponential distribution, Eq.6, predicted from the

Maxwell-Boltzmann distribution, with the slope $\underline{b} = (4/\sqrt{\pi})x_0$. For a ratio $F/B_{corr} \approx 5$, $x_0 = (\sqrt{\pi}/4)\ln F/B = 0.71$, from which the kinetic energy of the recoil nucleus $T_{A_t}*$ is estimated to be ≈30% of its excitation energy E^*.

F/B Ratios via Kinematics of Quasi-Elastic Scattering:

The F/B ratio given by Eq.5, when expressed explicity in terms of $T_{A_t}*$ and E^*, is

$$F/B = \frac{1 + \text{erf}\sqrt{3T_{A_t}*(\theta)/2E^*}}{1 - \text{erf}\sqrt{3T_{A_t}*(\theta)/2E^*}} \quad . \qquad \text{(Eq.7)}$$

At a scattering angle θ, the F/B ratio of the fragments emitted from the excited target recoil is kinematically determined, since, at angle θ, the excitation energy is fixed by the angle of deflection of the excited projectile nucleus. Curves of the values of F/B ratios of particles emitted from moving $^{94}A_t^*$ systems, evaluated from Eq.7, are plotted in Fig. 9 as a function of $\theta_{A_t}* \leq 70°(\text{lab})$ for excitation energies $E^* = 4.1$, 5.8 and 7.5 GeV specified by the measured angles $\bar{\theta}_{PF}$ at $\bar{\theta}_{TF}$ (Fig. 8 and Table I(b)). Plotted in Fig. 9 are the observed values of $\bar{\theta}_{TF}$ based on all events [circle], events with $\theta_{TF} \leq \theta(\text{med})$ [square] and with $\theta_{TF} > \theta(\text{med})$ [triangle]. By equating the observed angles $\bar{\theta}$ of the principal vectors $\hat{r}$ of the projectile and target fragments with θ_U* and $\theta_{A_t}*$, respectively, the F/B ratios are kinematically fixed.

If we focus specifically on the result deduced from all events (circle), the value $\bar{\theta}_{TF} = 47.1 \pm 2.1°$, when projected onto the calculated curve for $E^* = 5.8$ GeV gives a predicted value of $F/B = 5.44 \pm \frac{0.74}{0.63}$. The error in F/B is estimated from the statistical error in $\bar{\theta}_{TF}$ only. A better estimate of

the error in F/B is indicated by the hatched area that is bounded by the $\pm 1\sigma$ contours of $\bar{\theta}_{TF}$ and E^{*}(= 5.8 ± 0.5 GeV), the latter error being estimated from the statistical uncertainty in $\bar{\theta}_{PF}$ (i.e. the error associated with $\bar{\theta}_{U}*$, Fig. 8).

In Figs. 10a,b,c we compare the observed F/B_{corr} ratios (the hatched areas) with the calculated values for a) all events, b) events for which $\theta_{TF} \leq \theta_{TF}$ (med) = 44.9° and c) events for which $\theta_{TF} > \theta_{TF}$ (med), given in Table I(b). The calculated values plotted with closed symbols have used all projectile fragments $Z \geq 2$ to evaluate the angle $\bar{\theta}_{PF}$. The agreement between experiment and calculated values is good for the composite data and for the case where the target-fragment angles are $\bar{\theta}_{TF} \leq \theta_{TF}$(med), Figs. 10a and b, respectively. For angles greater than θ_{TF}(med) the predicted F/B ratio appears to differ significantly from experiment. However, the predicted value has a large error associated with it. The reason for this is apparent in Fig. 9; namely, the calculated F/B ratios become highly sensitive to the value of $\theta_{A_t}*$ at large angles, increasing rapidly when $\theta_{A_t}* \gtrsim 50°$ for the representative excitation energies.

As a further check on the internal consistency of our data, we also evaluated a mean angle $\bar{\theta}_{PF}$ based on heavy fragments, $Z \geq 6$, alone. The motivation here was to determine whether or not the lighter projectile fragments $2 \leq Z \lesssim 6$, which tend to be emitted at larger angles, had introduced large statistical fluctuations in the estimates of $\bar{\theta}_{PF}$. This possibility arises because $\bar{\theta}_{PF}$ is based on angle measurements only, with momenta unknown. By restricting the data to projectile fragments $Z \geq 6$ we partially alleviate this effect by limiting measurements to the high-momentum fragments, thereby eliminating any possibility for including mis-

identified target fragments in the sample of PFs. We also gain some insight on the problem of actually equating $\bar{\theta}_{PF}$ with the deflection angle of the projectile nucleus, θ_U*.

The results of these latter measurements are given in Table I(a). Within the statistical accuracies, the results derived for cases $Z_{PF} \geq 2$ and $Z_{PF} \geq 6$ are in basic agreement. The values of F/B (calc) evaluated from the data based in the emission angles of projectile fragments $\dot{Z} \geq 6$ are given in Table I(b) and plotted as open symbols in Fig. 10. Although the F/B ratios tend to give slightly better agreement with experiment then those based on projectile fragments $Z \geq 2$, it is clear that the calculated F/B ratios, based on values of $\bar{\theta}_{PF}$ obtained under the two charge-grouping criteria for PF's, are statistically consistent.

V. CONCLUSIONS

A topological examination of high-multiplicity events of 0.85 A GeV-^{238}U nuclei with Ag(Br) target nuclei in emulsion reveals that these interactions have kinematic features that are indicative of quasi-elastic reactions, e.g. $^{238}U + {}^{94}A_t \rightarrow {}^{238}U^* + {}^{94}A_t^*$, where the product nuclei, each with excitation energy E^*, are the effective sources for the projectile and target fragments. By equating the mean angles of emission of the projectile and target fragments, as given by their respective principal vectors $\hat{r}_{PF}$ and $\hat{r}_{TF}$, with the kinematically calculated angles of the (excited) product nuclei, estimates of the excitation energies E^* can be made. The resultant velocities of the U^* and A_t^* systems (in the direction of the principal vectors $\hat{r}$), when taken to be the source velocities of the projectile and target fragments, are in agreement with the source velocities deduced from the angular distributions of the projectile and target fragments.

By invoking a Maxwell-Boltzmann distribution to describe the emission of the target fragments from a moving source, a predicted F/B asymmetry in the emission of the TFs relative to their principal vector is kinematically determined. A comparison of the kinematically calculated values of the F/B ratio of the target fragment with those observed in this experient showed a marked agreement between them.

Thus, while all the characteristic velocities (to the extent they could be inferred from measurements of the angular distributions and their means of the projectile and target fragments) were all in agreement with those predicted from the quasi-elastic-fragmentation (QEF) model, it is clear that to test the model further requires data augmented with charge and momentum information.

Conceptually, the QEF model encompasses momentum and energy conservation germane to two-body kinematics. The notion that the product nuclei can be considered as coherent, excited nuclear systems interacting as collective aggregates contrasts with models that view interacting nuclei in terms of, for example, nucleon-nucleon cascades and nuclear fluid hydrodynamics. Yet, experimental evidence is mounting for the existence of significant collective "bounce-off" effects in collisions between heavy nuclei. The event shown in Fig. 1 gives strong visual evidence for such collective effects--in both the projectile- and target-related fragments. As in a broad range of applications, the assumption of a thermalized Maxwell-Boltzmann distribution to interrelate the observed angular distribution of the target fragments with the longitudinal and excitation energies of the emitting system can only be justified, as, indeed, can the model itself, by its simplicity and by the fact that it gives reasonable account of experiment.

ACKNOWLEDGMENTS

The authors thank H.J. Crawford and P.J. Lindstrom for their valuable and constructive comments on this work. We appreciate the scanning/measuring efforts of Santa Chatterji, Mohamed Ghoniem, Hester Yee, and Matt Bloomer, and the excellent support given us by the Operations Staff of the Bevalac.

This work was supported by the Director, Office of Energy Research, Division of Nuclear Physics of the Office of High Energy and Nuclear Physics of the U.S. Department of Energy under Contract DE-AC03-76SF00098.

References

1) E.M. Friedlander, H.H. Heckman, and Y.J. Karant, Phys. Rev. C 27, 2436 (1983).

2) H.A. Gustafsson, H.H. Gutbrod, B. Kolb, H. Löhner, B. Ludewigt, A.M. Poskanzer, T. Renner, H. Riedesel, H.G. Ritter, A. Warwick, F. Weik, and H. Wieman, Phys. Rev. Lett. 52, 1950 (1984).

3) R.E. Renfordt, D. Schall, R. Bock, R. Brockmann, J.W. Harris, A. Sandoval, R. Stock, H. Ströbele, D. Bangert, W. Rauch, G. Odyniec, H.G. Pugh, and L.S. Schroeder, Phys. Rev. Lett. 53, 763 (1984).

4) G. Buchwald, G. Graebner, J. Theis, J. Maruhn, W. Greiner, and H. Stöcker, Phys. Rev. Lett. 52, 1594 (1984). See also H. Stöcker, AIP Special Report, in Physics Today 39, S-49 (1986).

5) J. Gosset, H.H. Gutbrod, W.G. Meyer, A.M. Poskanzer, A. Sandoval, R. Stock, and G.D. Westfall, Phys. Rev. C 16, 629 (1977).

6) H.H. Heckman, H.J. Crawford, D.E. Greiner, P.J. Lindstrom, and L.W. Wilson, Phys. Rev. C 17, 1651 (1978).

Table I: a) Summary of experimental data. b) Excitation energies and F/B ratios from kinematic model based on angle data a).

			All Events	$\theta_{TF} \leq \theta_{TF}(med)$	$\theta_{TF} > \theta_{TF}(med)$
	$\bar{\theta}_{TF}$(deg)		47.1 ± 2.1	35.8 ± 1.3	58.9 ± 2.4
a)	$\bar{\theta}_{PF}$	$Z_{PF} \geq 2$	2.35 ± 0.20	1.94 ± 0.21	2.78 ± 0.31
		$Z_{PF} \geq 6$	2.09 ± 0.19	2.34 ± 0.32	1.81 ± 0.70
	F/B	obs	5.94 ± 0.51	6.21 ± 0.73	5.64 ± 0.71
		corr	5.28 ± 0.46	5.52 ± 0.66	5.01 ± 0.65
b)	E^*(GeV)	$Z_{PF} \geq 2$	5.8 ± 0.5	7.5 ± 0.7	4.1 ± 0.5
		$Z_{PF} \geq 6$	5.4 ± 0.5	8.6 ± 1.0	3.1 ± 0.7
	F/B_{Kin}	$Z_{PF} \geq 2$	$5.44^{+0.74}_{-0.63}$	4.62 ± 0.20	$8.56^{+8.44}_{-2.21}$
		$Z_{PF} \geq 6$	$4.90^{+0.70}_{-0.46}$	$5.51^{+0.31}_{-0.29}$	$4.84^{+1.26}_{-0.70}$

Figure Captions

Fig. 1 Micro-projection drawing of a U + Ag(Br) event in emulsion that is characteristic of a high-multiplicity, but peripheral, interaction. The visually apparent asymmetries in the emission angles of the projectile (forward cone) and target fragments are the prominent features of this class of event.

Fig. 2 a) Beam frame: $\underline{i}$-axis is directed along beam direction, $\underline{j}$-axis lies in plane of emulsion. Polar and azimuth angles of fragment vector r are θ and ϕ, respectively.

b) Fragment frames: Frame of reference established by principal vectors $\hat{r}$ of the projectile and target fragments, as defined in text. Illustration shows target fragment frame, where the angle θ'_{TF} of the target-fragment vector r is given relative to $\hat{r}_{TF}$, the latter at $\bar{\theta}_{TF}$ in the beam frame.

Fig. 3 Scatter plot and marginal distributions of the multiplicities of the projectile and target fragments for the selected events in this experiment. Criteria were: i) projectile fragments: $N_{PF} \geq 8$, $Z \geq 2$ and ii) target fragments: $N_{TF} \geq 10$, $Z \geq 1$. Mean multiplicities are $\bar{N}_{PF} = 13.5$ ($D = 3.6$) and $\bar{N}_{TF} = 22.7$ ($D = 5.8$).

Fig. 4 Differences between the azimuthal angles of the principal projectile and target vectors, $\hat{r}_{PF}$ and $\hat{r}_{TF}$. a) Solid line: experimental distribution; b) Dashed line: Monte-Carlo generated distribution, based on isotropic emission of the projectile and target fragments.

Fig. 5 Angular distributions for the principal vectors $\hat{r}$ of the projectile fragments ($Z \geq 2$) and target fragments. The mean angles of emission of these vectors are: $\bar{\theta}_{PF} = 2.35 \pm 0.20°$, $\bar{\theta}_{TF} = 47.1 \pm 2.1°$.

Fig. 6 Projected angular distribution of $Z = 2$ projectile fragments in the projectile-fragment frame. The dispersion of the distribution is $D = 3.6°$ (63 mrad).

Fig. 7 Angular distributions of the target fragments in the target-fragment frame. a) closed circles: experimental data; slope of line through data is to $\underline{b} = \ell n\ (F/B_{obs}) = 1.78 \pm 0.09$. b) dashed line: input distribution to Monte-Carlo calculation having slope $\underline{b} = \ell n\ (F/B_{corr}) = 1.66$ that reproduces the experimental data a).

Fig. 8 Kinematics of the reaction $^{238}U(0.85\ A\ GeV) + {}^{94}A_t \rightarrow {}^{238}U^* + {}^{94}A_t^*$, giving the emission angles of the product nuclei as a function of excitation energy $E^*(GeV)$, under the assumption the final masses are $M^* = M + E^*$ GeV, with $M = 0.9315$ A GeV. Data points are: circle, all events; square, events with $\theta_{TF} \leq \theta_{TF}$ (med) where θ_{TF} (med) = 44.9°; and triangle, $\theta_{TF} > \theta_{TF}$(med).

Fig. 9 Model-calculated curves of F/B ratios of particles emitted from moving A_t^* systems (Eq.7) for excitation energies E^* = 4.1, 5.8 and 7.5 GeV. Data points are as defined in Fig. 8.

Fig. 10 Comparison of experimental and calculated F/B ratios. Experimental data F/B_{corr} (diamond with hatch areas) are given for

a) the composite data, all PFs and TFs included,

b) data sample with $\theta_{TF} \leq \theta_{TF}(med)$ and

c) data sample with $\theta_{TF} \geq \theta_{TF}(med)$.

The calculated F/B ratios plotted in a,b,c) (with error estimates) are shown as solid points when $\bar{\theta}_{PF}$ is based on the criteria $Z_{PF} \geq 2$, and as open points when $Z_{PF} \geq 6$.

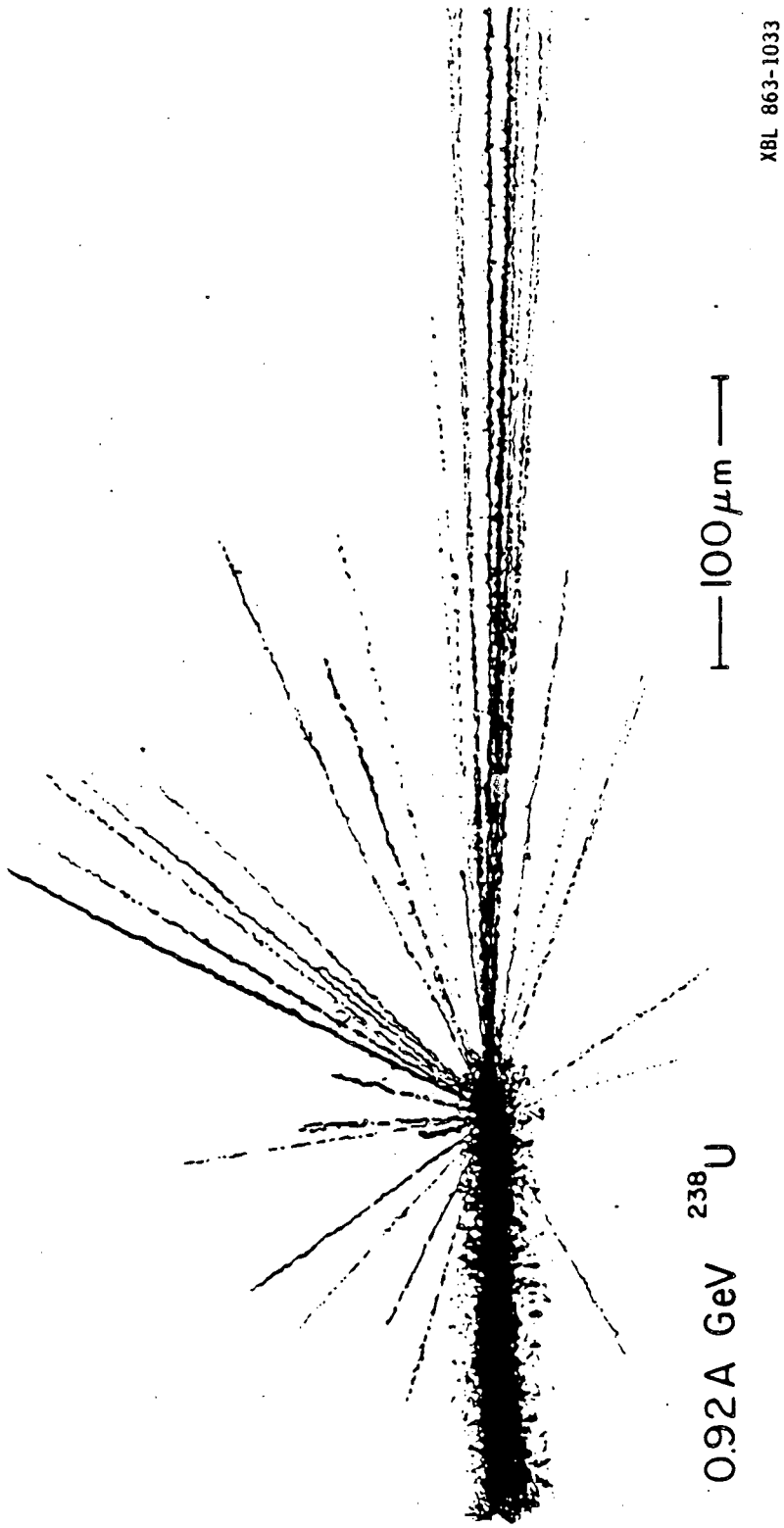

Fig. 1

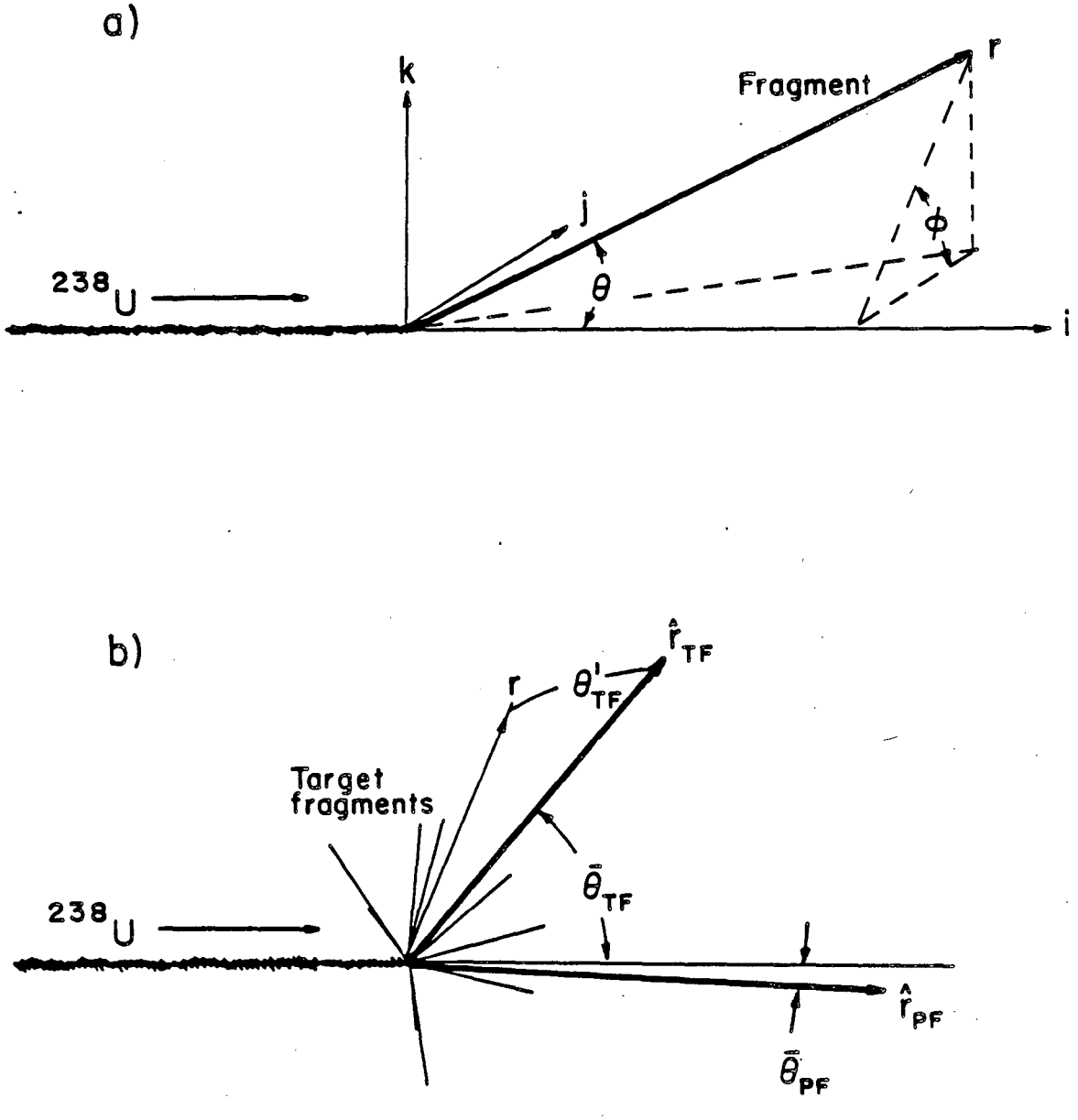

XBL 863-834

Fig. 2

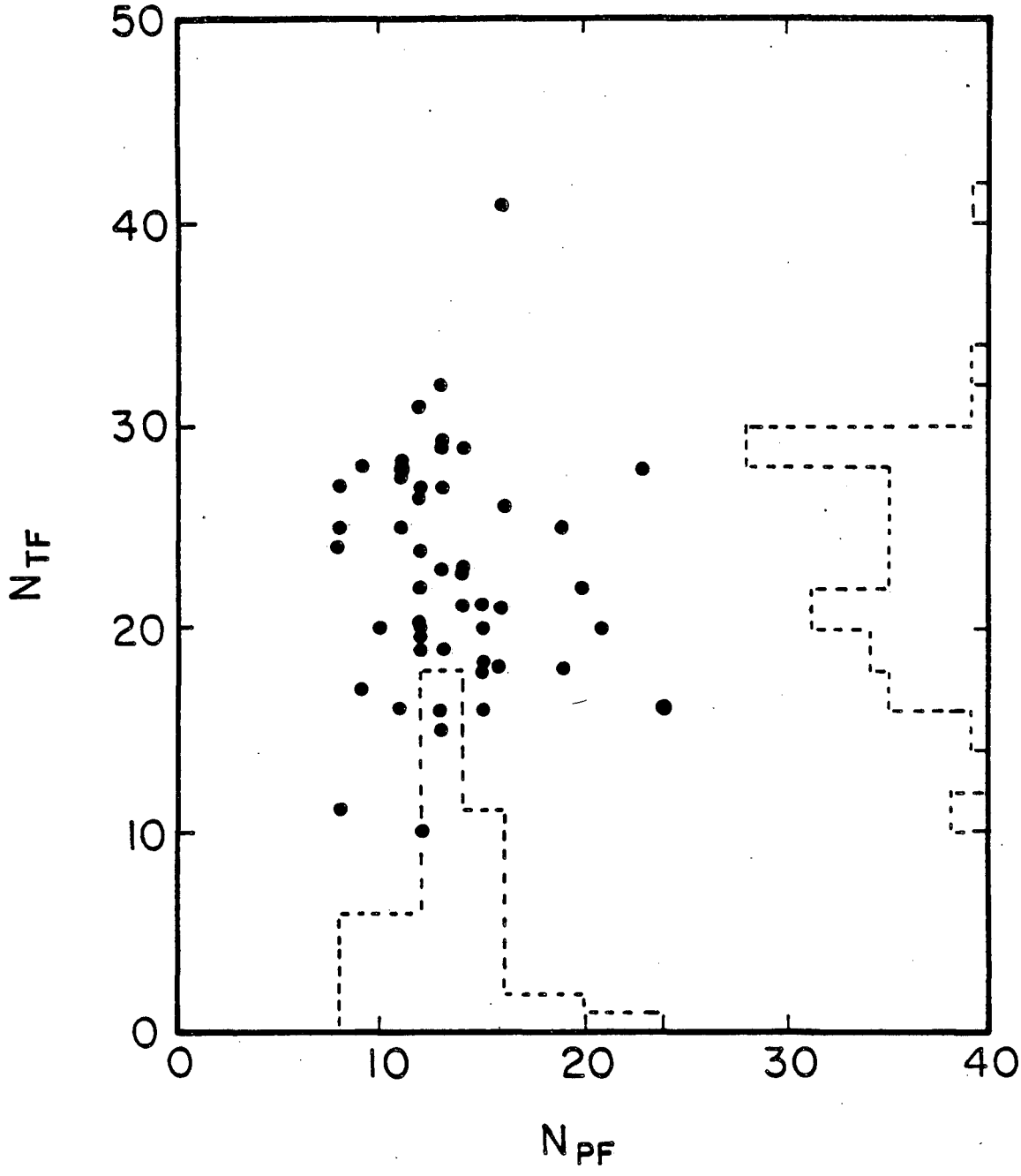

XBL 863-835

Fig. 3

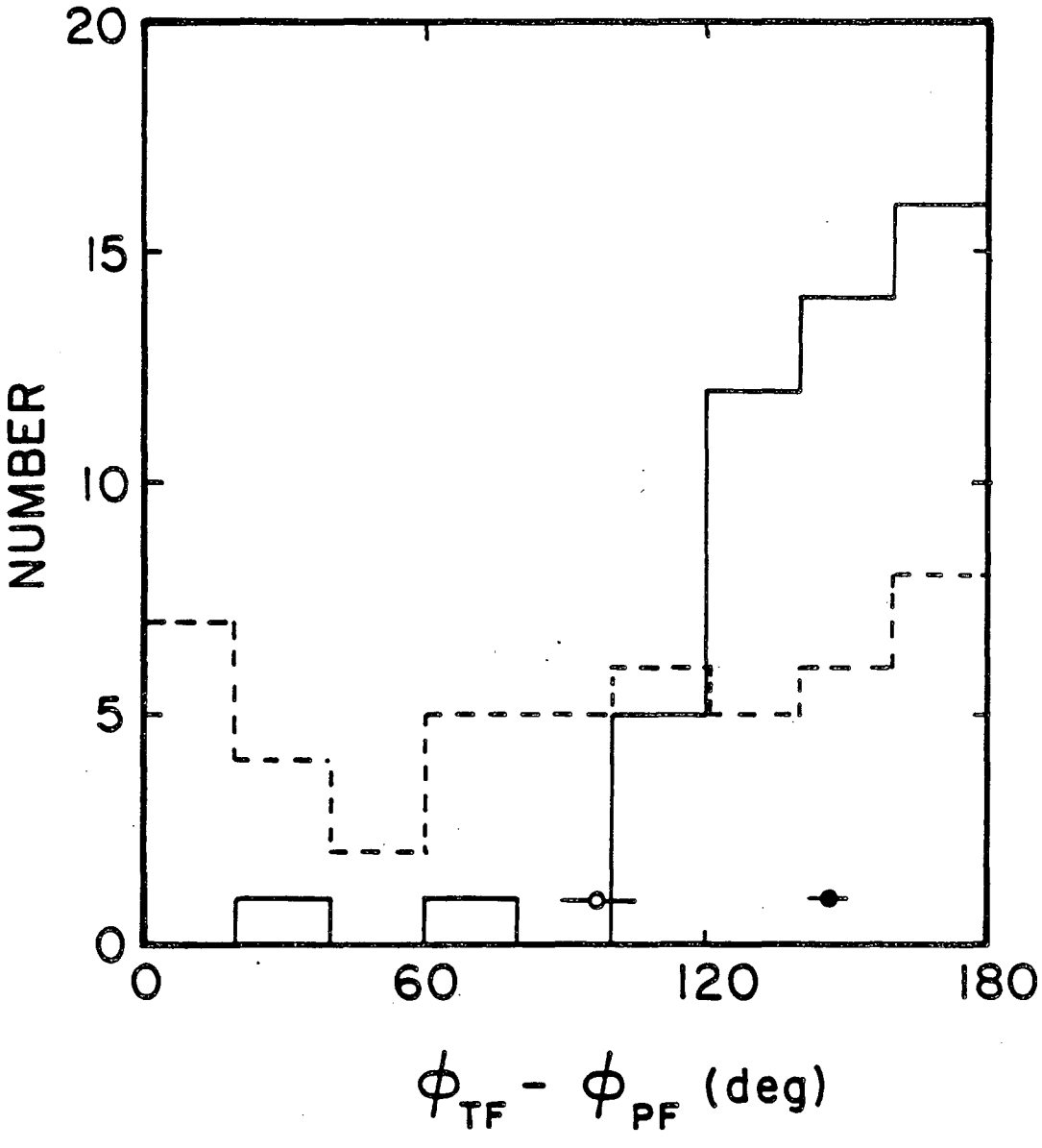

XBL 863-836

Fig. 4

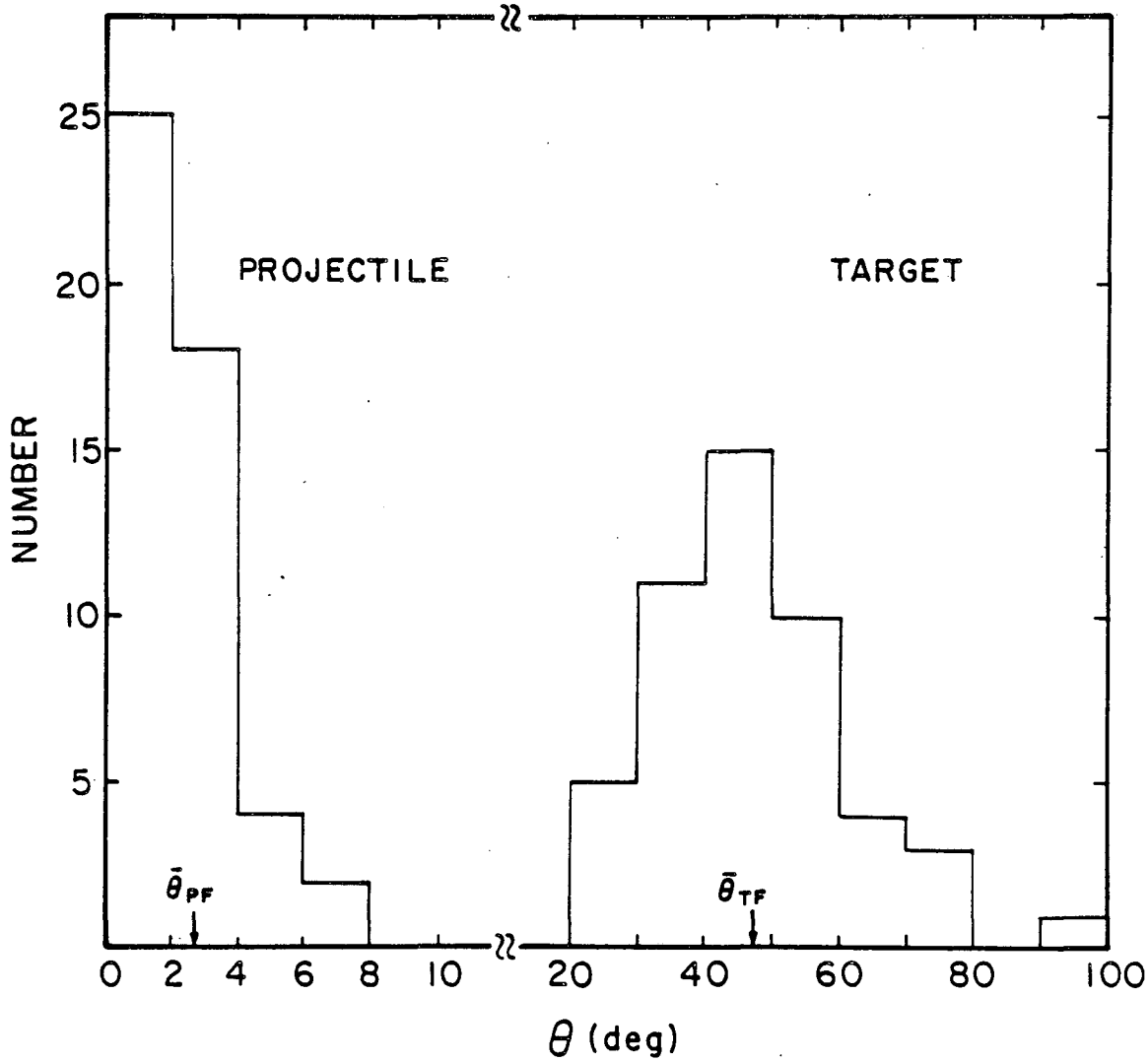

XBL 863-837

Fig. 5

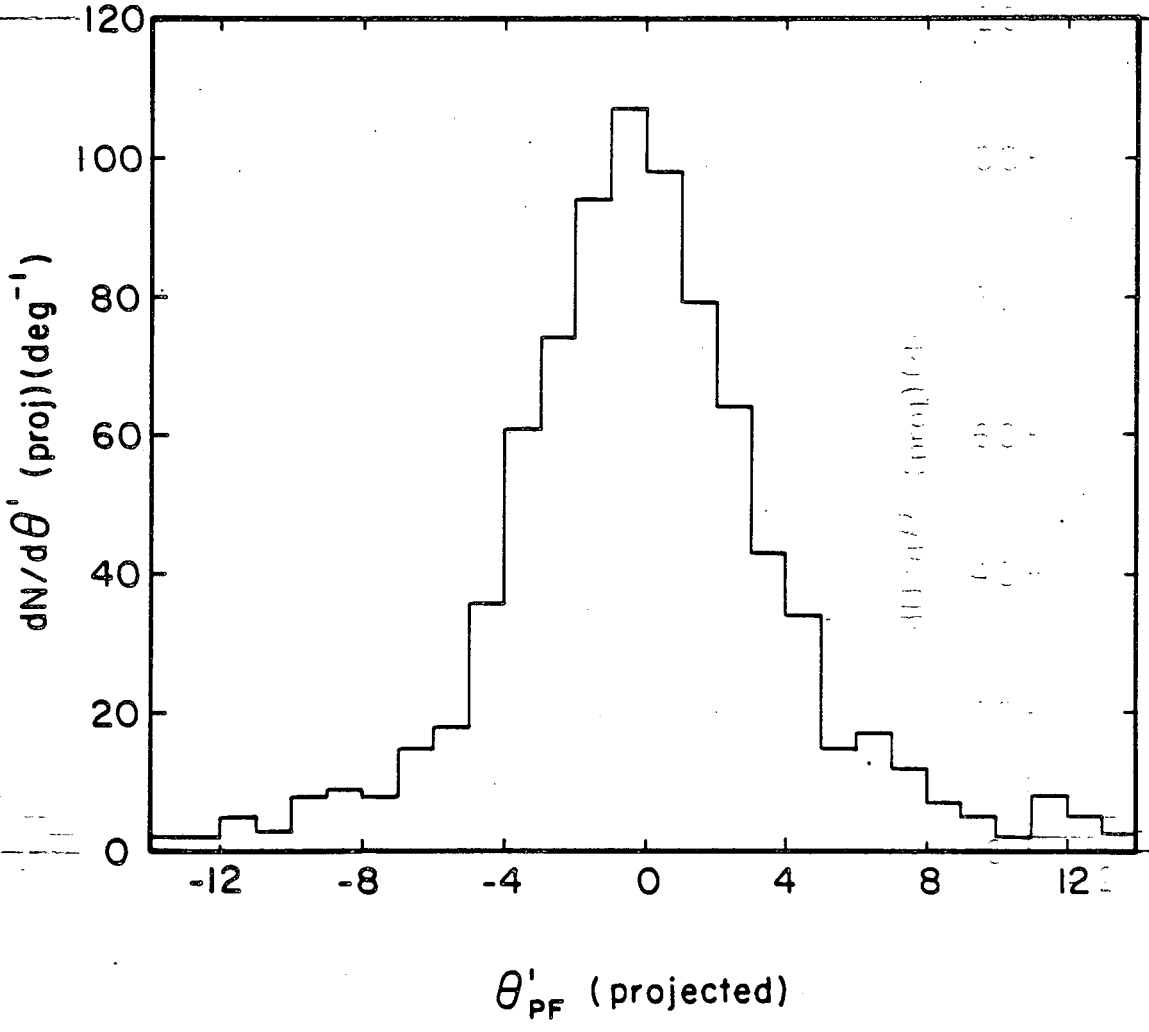

XBL 863-838

Fig. 6

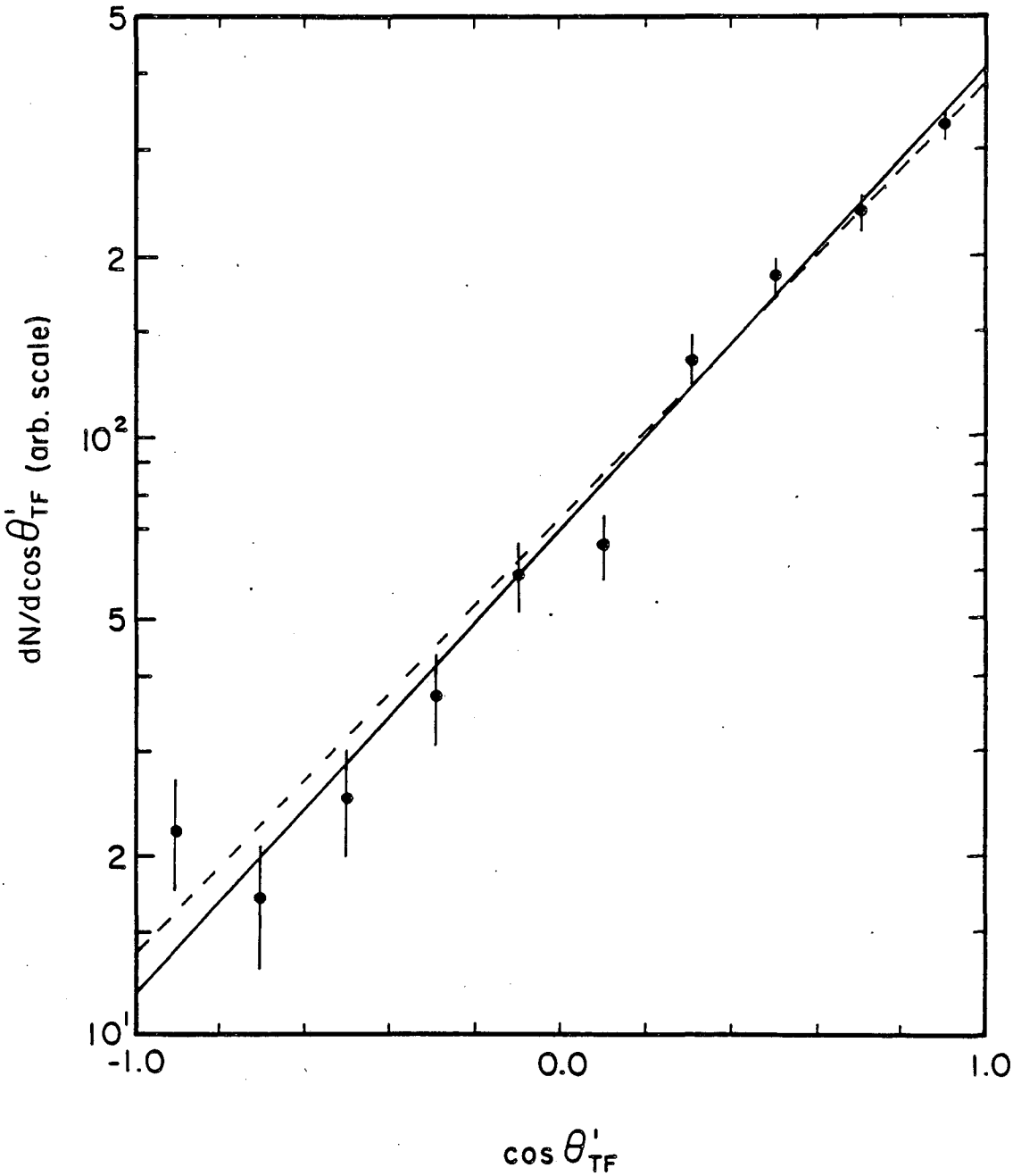

XBL 863-839

Fig. 7

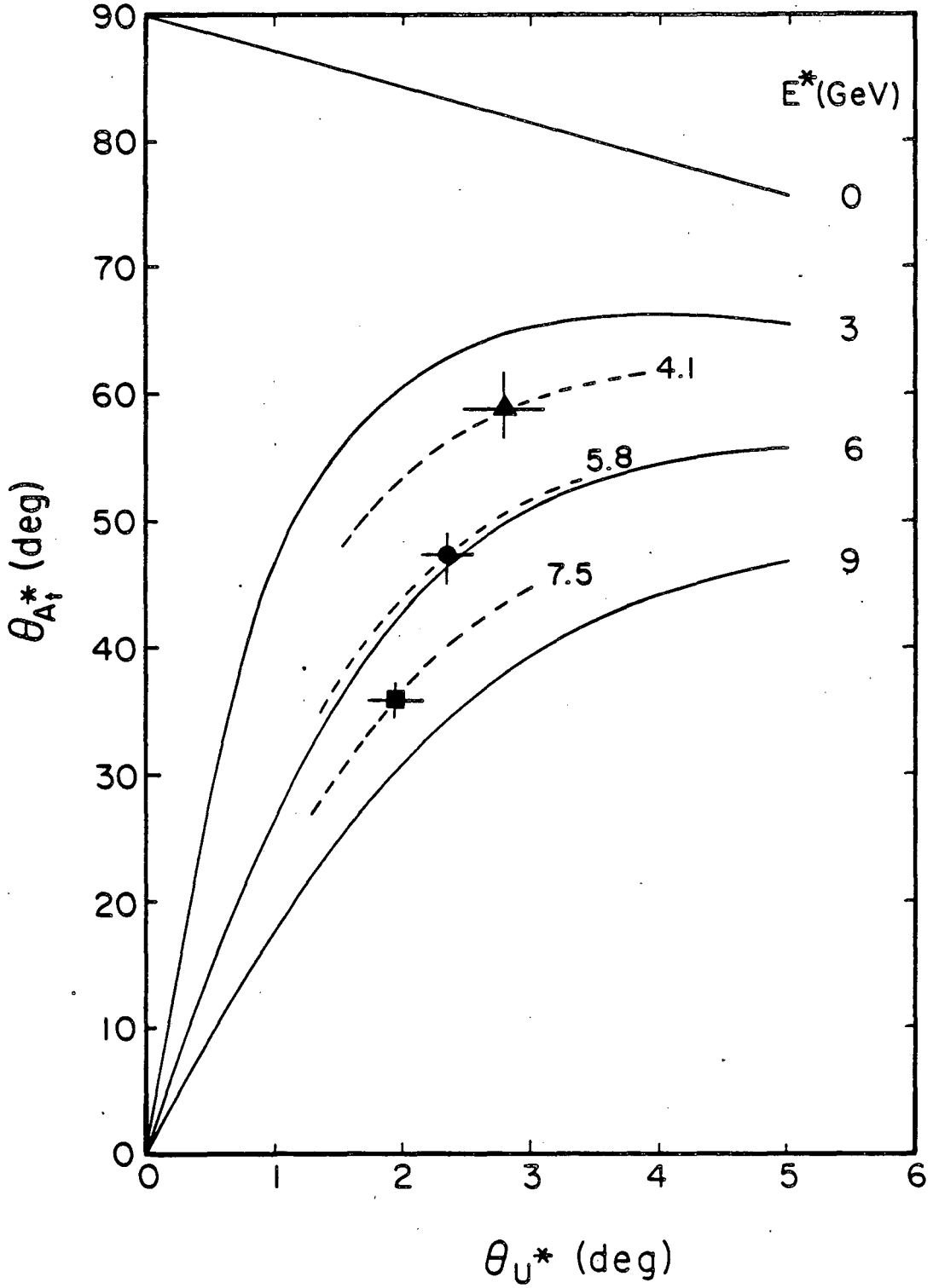

XBL 863-840

Fig. 8

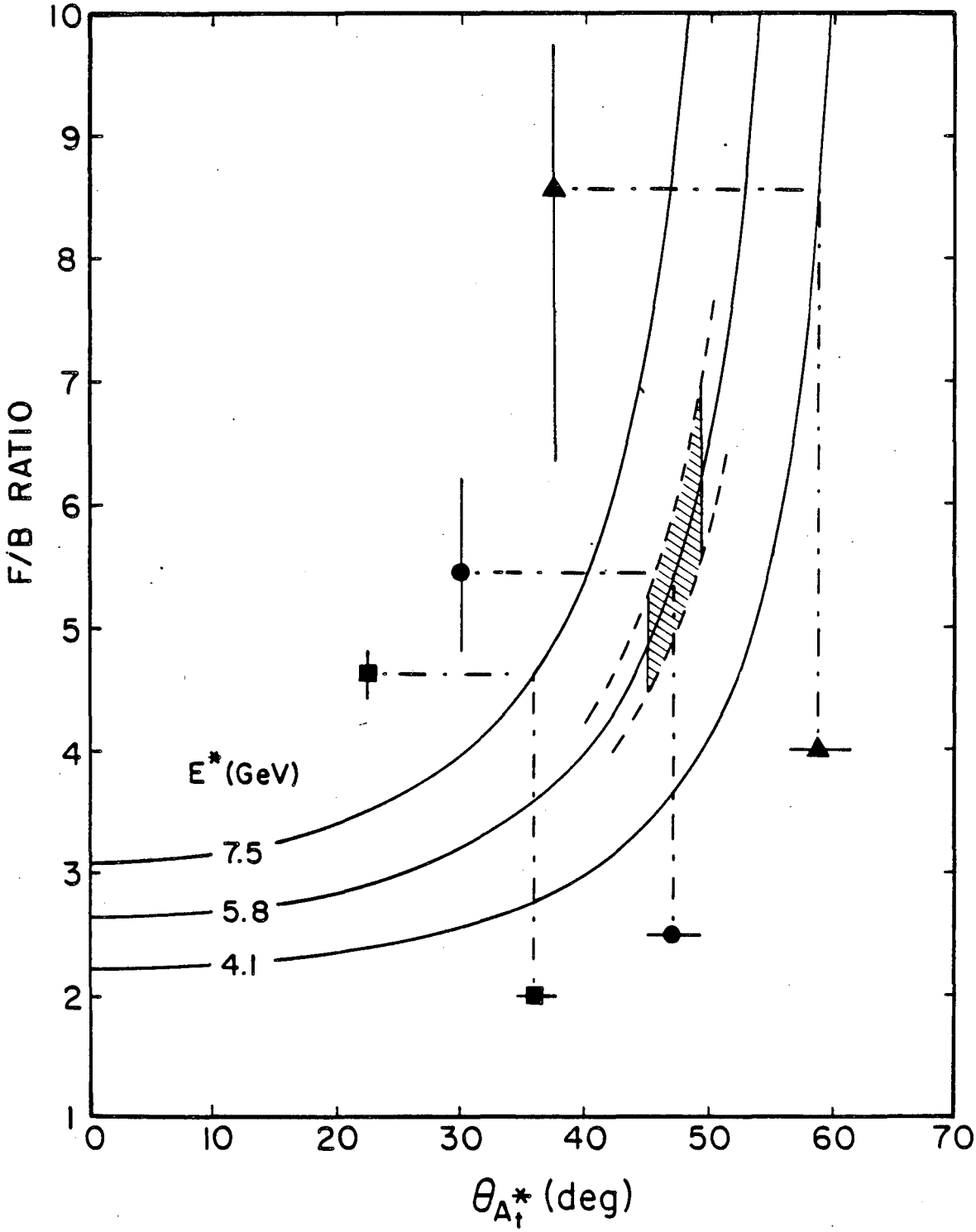

XBL 863-841

Fig. 9

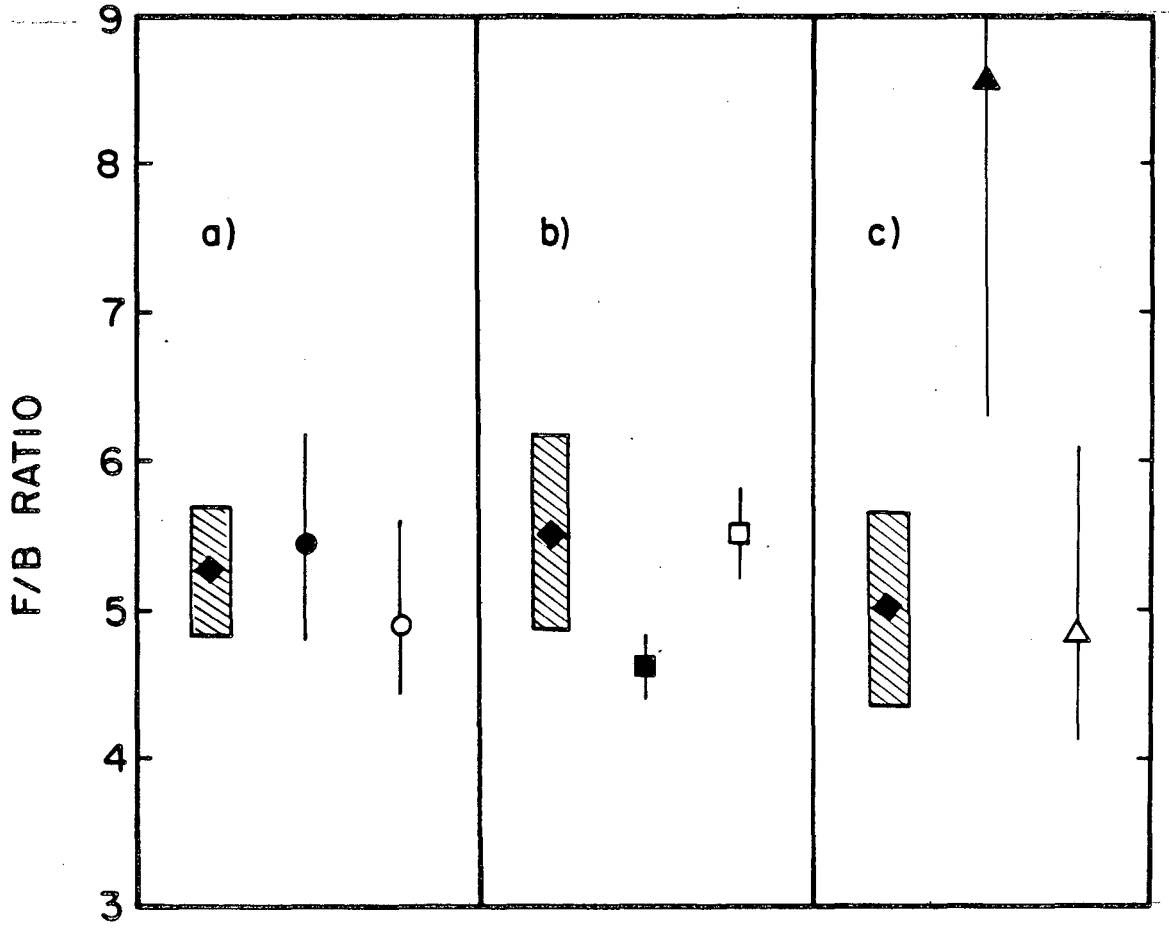

XBL 863-842

Fig. 10

This report was done with support from the Department of Energy. Any conclusions or opinions expressed in this report represent solely those of the author(s) and not necessarily those of The Regents of the University of California, the Lawrence Berkeley Laboratory or the Department of Energy.

Reference to a company or product name does not imply approval or recommendation of the product by the University of California or the U.S. Department of Energy to the exclusion of others that may be suitable.

LAWRENCE BERKELEY LABORATORY
TECHNICAL INFORMATION DEPARTMENT
UNIVERSITY OF CALIFORNIA
BERKELEY, CALIFORNIA 94720